nature materials

LETTERS

PUBLISHED ONLINE: 13 MARCH 2011 | DOI: 10.1038/NMAT2978

Air-stable magnesium nanocomposites provide rapid and high-capacity hydrogen storage without using heavy-metal catalysts

Ki-Joon Jeon[1†], Hoi Ri Moon[2†‡], Anne M. Ruminski[2], Bin Jiang[3], Christian Kisielowski[4], Rizia Bardhan[2] and Jeffrey J. Urban[2*]

Hydrogen is a promising alternative energy carrier that can potentially facilitate the transition from fossil fuels to sources of clean energy because of its prominent advantages such as high energy density (142 MJ kg^{-1}; ref. 1), great variety of potential sources (for example water, biomass, organic matter), light weight, and low environmental impact (water is the sole combustion product). However, there remains a challenge to produce a material capable of simultaneously optimizing two conflicting criteria—absorbing hydrogen strongly enough to form a stable thermodynamic state, but weakly enough to release it on-demand with a small temperature rise. Many materials under development, including metal–organic frameworks[2], nanoporous polymers[3], and other carbon-based materials[4], physisorb only a small amount of hydrogen (typically 1–2 wt%) at room temperature. Metal hydrides were traditionally thought to be unsuitable materials because of their high bond formation enthalpies (for example MgH_2 has a $\Delta H_f \sim 75$ kJ mol^{-1}), thus requiring unacceptably high release temperatures[5] resulting in low energy efficiency. However, recent theoretical calculations[6,7] and metal-catalysed thin-film studies[8] have shown that microstructuring of these materials can enhance the kinetics by decreasing diffusion path lengths for hydrogen and decreasing the required thickness of the poorly permeable hydride layer that forms during absorption. Here, we report the synthesis of an air-stable composite material that consists of metallic Mg nanocrystals (NCs) in a gas-barrier polymer matrix that enables both the storage of a high density of hydrogen (up to 6 wt% of Mg, 4 wt% for the composite) and rapid kinetics (loading in <30 min at 200 °C). Moreover, nanostructuring of the Mg provides rapid storage kinetics without using expensive heavy-metal catalysts.

There have been various efforts to synthesize nanosized magnesium, such as ball-milling[9], sonoelectrochemistry[10], gas-phase condensation[11] and infiltration of nanoporous carbon with molten magnesium[12]. However, these approaches remain limited by inhomogeneous size distributions and high reactivity toward oxygen. Our synthesis for air-stable alkaline earth metal NC/polymer composites consists of a one-pot reduction reaction of an organometallic Mg^{2+} precursor in the presence of a soluble organic polymer chosen for its hydrogen gas selectivity (Fig. 1). The Mg NCs/PMMA nanocomposites were synthesized at room temperature from a homogeneous tetrahydrofuran (THF) solution containing the following dissolved components: the organometallic precursor bis(cyclopentadienyl)magnesium (Cp_2Mg), the reducing agent lithium naphthalide, and the gas-selective polymer poly(methyl methacrylate) (PMMA). Mg nanocrystals are then nucleated and grown in this solution by means of a burst-nucleation and growth mechanism[13] in which lithium naphthalide reduces the organometallic precursor in the presence of a capping ligand (the soluble PMMA ($M_w = 120{,}000$) acts as a capping ligand for the Mg nanocrystals)[14]. Transmission electron microscopy (TEM) analysis of our reaction mixture before addition of reductant, immediately thereafter, and at later stages of the growth (Supplementary Fig. S1) further support this model.

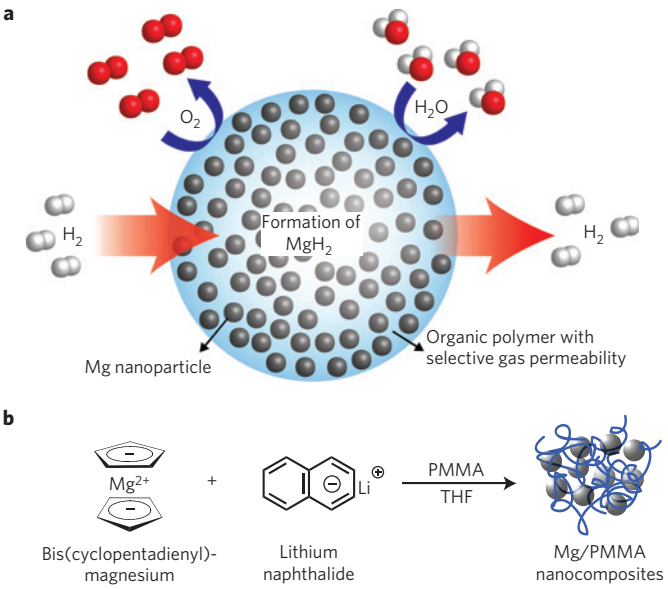

Figure 1 | Mg NCs in a gas-barrier polymer matrix. a, Schematic of hydrogen storage composite material: high-capacity Mg NCs are encapsulated by a selectively gas-permeable polymer. **b**, Synthetic approach to formation of Mg NCs/PMMA nanocomposites.

[1]Environmental Energy Technologies Division, Lawrence Berkeley National Laboratory, Berkeley, California 94720, USA, [2]The Molecular Foundry, Material Science Division, Lawrence Berkeley National Laboratory, Berkeley, California 94720, USA, [3]FEI Company, NE Dawson Creek Dr., Hillsboro, Oregon, 97124, USA, [4]National Center for Electron Microscopy and Helios SERC, Lawrence Berkeley National Laboratory, Berkeley, California 94720, USA. †These authors contributed equally to this work. ‡Present address: Interdisciplinary School of Green Energy, Ulsan National Institute of Science and Technology (UNIST), Ulsan 689-798, Korea. *e-mail: jjurban@lbl.gov.

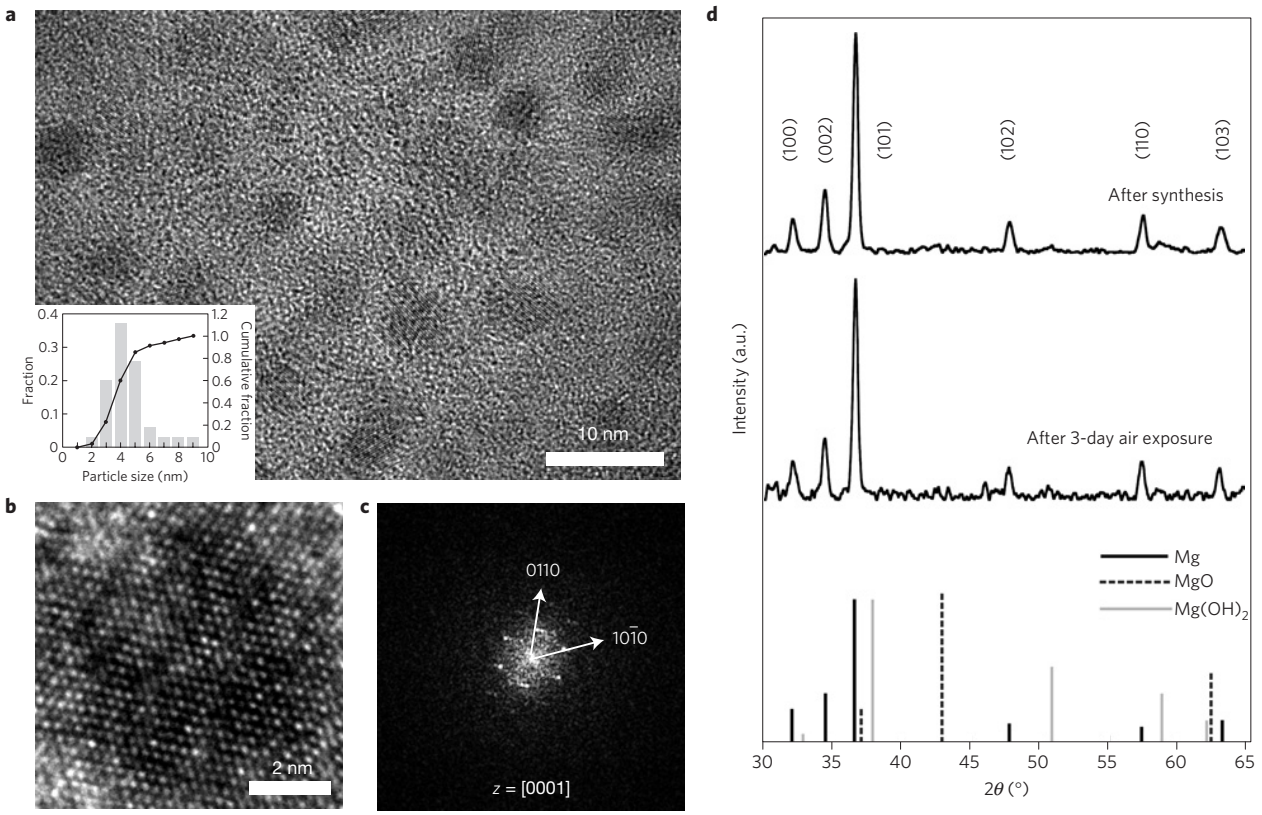

Figure 2 | Verification of single crystalline Mg nanoparticles. a, High-resolution TEM micrograph of as-synthesized Mg NCs/PMMA composites. Inset: Histogram and cumulative distribution function of Mg particle size distributions. The average Mg NC diameter is 4.9 ± 2.1 nm. **b**, Atomic-resolution image of a single Mg NC. **c**, Digital diffractogram of the Mg NC in **b**, revealing the presence of lattice fringes with a separation of 2.789 Å, in agreement with the (002) interplanar *d* spacing of hexagonal magnesium (JCPDS 04-0770, 2.7782 Å). Further analysis shows evidence of a slight trigonal distortion in some of the nanocrystals studied. **d**, X-ray diffraction patterns of Mg NCs/PMMA composites: as-synthesized (top), and after three days of air-exposure (middle) with reference diffraction patterns (bottom) of hexagonal Mg (solid black line, JCPDS 04-0770), cubic MgO (dashed black line, JCPDS 89-7746), and hexagonal $Mg(OH)_2$ (pale grey line, JCPDS 07-0239). Peaks located at $2\theta = 32.2°$, 34.4°, 36.6°, 47.8°, 57.4° and 63.1° are assigned to the (100), (002), (101), (102), (110), and (103) planes of hexagonal magnesium, respectively. The highest intensity $Mg(OH)_2$ peak after 3 days of air exposure, occurring at $2\theta = 58.6$ (110), is 1/30th the intensity of the most intense Mg peak (101), and only two times the intensity of the root-mean-squared baseline noise intensity.

This synthesis provides a gas-selective polymer barrier for the Mg NCs, which enables them to absorb and release hydrogen without oxidizing. This is vital, as magnesium metal exothermically (-601.24 kJ mol^{-1}) forms oxides on exposure to even minute quantities of air or water, resulting in MgO and $Mg(OH)_2$ layers which, in addition to not absorbing hydrogen, also actively block penetration of H_2 molecules and H atoms. Thus oxidation deleteriously creates 'dead' layers, inactive as storage media. Although nanocrystals potentially provide a route to boosting the kinetics of hydrogenation in metallic Mg because of the intrinsically short diffusion paths for hydrogen, no methods have yet been demonstrated to effectively protect even ligand-passivated Mg NCs from oxidation[15]. For our composites, we chose the polymer, poly(methyl methacrylate) (PMMA; ref. 16) which shows the ability to mitigate oxygen penetration and damage, with permeabilities for H_2 and O_2 of 1.15 and 0.0269×10^5 mol m^{-1} s^{-1} Pa^{-1} (3.70 and 0.0863×10^{10} (cm^3(STP) cm)/(cm^2 s cmHg)), respectively[17], resulting in a H_2/O_2 permeability ratio of 42.9 at 35 °C, far exceeding that of other commonly available polymers (for example, 1.03 at 35 °C and 8.57 at 25 °C for poly(dimethylsiloxane) and polycarbonate, respectively)[16–18]. Additionally, it is critical to have a mechanically flexible polymer, both to optimize volumetric storage capacity by eliminating 'dead space' as well as providing an accommodating support for the large volume expansion (33% for the Mg to MgH_2 transition) that metals undergo during absorption cycling[19].

TEM micrographs showed that PMMA embedded Mg NCs have an approximately spherical morphology (Fig. 2a) with an average diameter of 4.9 ± 2.1 nm and are well-distributed throughout the polymer phase with no evidence of agglomeration (Supplementary Figs S2 and S3). Although TEM analysis of more than 100 NCs from more than 12 different syntheses did not reveal larger NCs, the crystalline sizes of the Mg NCs determined from the X-ray diffraction (XRD) data are about 15 ± 2 nm (Supplementary Table S1), which indicates the possibility of either a bimodal distribution of Mg NCs (~5 and ~15 nm) or agglomeration, although neither of these has been observed by means of microscopy. Figure 2b shows an atomic-resolution image of a particle along the [0001] direction which shows evidence of defects in the crystal lattice. Digital diffractograms obtained from TEM images taken of Mg NCs/PMMA composites exposed to air for two weeks remarkably display diffraction only from hexagonal crystalline magnesium (Fig. 2c); there is no evidence for detectable amounts of a magnesium oxide layer. X-ray diffraction patterns (Fig. 2d) of the Mg NCs/PMMA composite taken immediately after synthesis, and after 3 days of air exposure at room temperature, display diffraction peaks of single-phase hexagonal magnesium and exceptionally minute intensity from peaks characteristic of MgO (ref. 20) and $Mg(OH)_2$, indicating impressive air stability against oxidation. This synthetic strategy was verified by embedding these Mg NCs in other organic materials such as hexadecylamine for

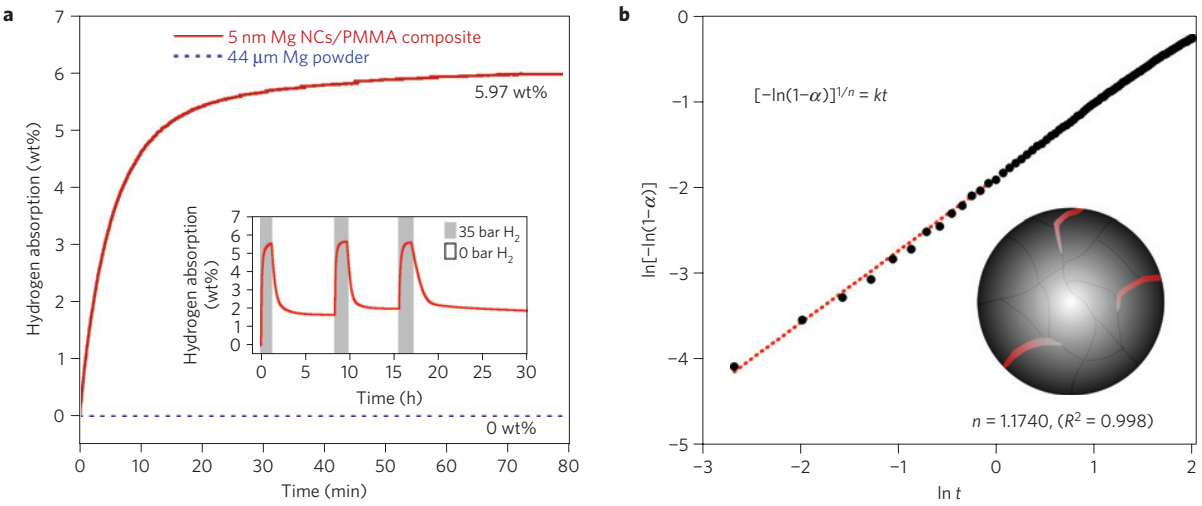

Figure 3 | Hydrogen absorption in Mg NCs/PMMA composites. a, Enhancement in hydrogen absorption properties of Mg NCs/PMMA composites (absorption at 200 °C and 35 bar) in comparison to bulk Mg. The Mg NCs/PMMA composites display a calculated hydrogen absorption capacity value of 5.97 wt% Mg (~4 wt% total). Inset: Hydrogen absorption/desorption cycling at 200 °C. **b**, The initial growth mechanism of MgH_2 in Mg NCs/PMMA composites. Hydrogen absorption data shown in **a** (initial 6 min) was used to correlate with a Johnson–Mehl–Avrami model (equation (1)).

comparison, and the resulting X-ray diffraction spectra indicate immediate oxidation (Supplementary Fig. S4). Thermogravimetric analysis of the Mg NCs/PMMA composites indicates that 61% of the total nanocomposite weight is hydrogen storage active material (Supplementary Fig. S5).

The hydrogen absorption capacity for Mg NCs/PMMA composites was measured in relation to a known reference material, bulk Mg (44 μm), using a Sieverts PCT-Pro at 35 bar H_2 and 200 °C (Fig. 3a). The bulk Mg shows no weight increase on hydrogen exposure, indicating a lack of MgH_2 formation. However, the Mg NCs/PMMA composites display a sharp weight increase on hydrogen exposure, with a steep slope of hydrogenation occurring during the first 6 min, which plateaus off to constant mass in <30 min. The differences in slope between the first 6 min and the remainder of the absorption curve are attributed to a change in the rate-limiting mechanism for hydrogen uptake[21]. It was found that the hydrogen absorption capacity of the Mg NCs/PMMA composite was well-preserved through three absorption/desorption cycles (Fig. 3a inset), however slightly decreased dehydriding kinetics were observed after the third cycle as evinced from the decreased slope of descent. This marginal degradation is probably due to material fatigue owing to relaxation of structural defects, but more detailed investigation is necessary. From the measured absorption isotherm, a calculated hydrogen absorption capacity value of 5.97 wt% Mg (~4 wt% in overall composite mass) is reported. Thus, these composites absorb 78.6% of the theoretical value of magnesium. The calculated experimental volumetric hydrogen capacity of the composites is 55 g l^{-1} (the theoretical capacity for the Mg NCs/PMMA composites is 70 g l^{-1}). This value exceeds the volumetric capacity of compressed hydrogen (10,000 psi, 30 g l^{-1}) by 180%, demonstrating that Mg NCs/PMMA composites provide a viable storage alternative to gas tanks. In comparison, bulk Mg (<37 μm) absorbs only ±2% of the theoretical hydrogen absorption value within 10 min at 35 bar, and requires prohibitively high temperatures (400 °C) to do so[22].

To verify that hydrogen uptake in this Mg NCs/PMMA composite is due to metal-hydride formation and not polymer adsorption, time-resolved low-loss electron energy loss spectroscopy (EELS) was performed on MgH_2 NCs/PMMA composites using a monochromated and aberration-corrected transmission electron microscope at 80 kV (ref. 23). Figure 4 displays the time resolved and normalized EELS spectrum of the

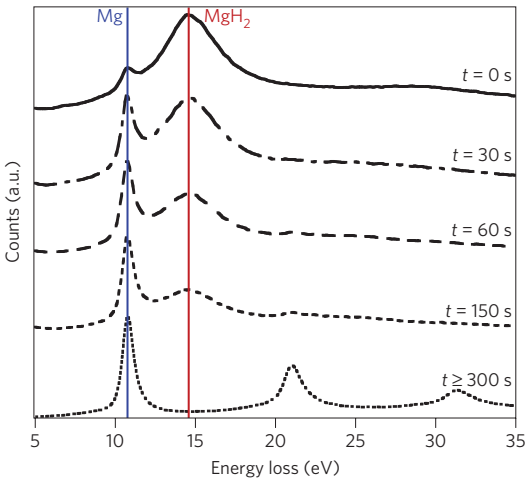

Figure 4 | Time-resolved monitoring of hydrogen desorption from MgH_2 NCs/PMMA composites. Low-loss EELS spectra of MgH_2 NCs/PMMA using the TEAM 0.5 microscope at 80 kV. Mg plasmon energy loss: 10.5 eV, and MgH_2 plasmon energy loss: 14.6 eV. All spectra were normalized to the Mg peak position at 10.5 eV. Note that peaks occurring at a constant interval of ~10.3 eV (located at 21.0 and 31.3 eV) are Mg plasmon replicas.

MgH_2 NCs/PMMA composites. At time 0 s, two distinct, intense EELS peaks are observed at 10.5 and 14.6 eV, corresponding to the co-existence of pure Mg and MgH_2, respectively[24]. As the exposure time to the electron beam increases, the relative intensity of the Mg peak increases in relation to the intensity of the MgH_2 peak. The intensity ratio (I_{MgH2}/I_{Mg}) reduces from 2.04 to 0 during the 5 min of beam exposure owing to hydrogen loss from the hydride phase. Notably, the presence of the characteristic MgO peak at about 22.3 eV (Supplementary Fig. S6) was not observed in the sample, further evidence supporting the remarkable oxidative stability of these composites.

Theoretical calculations indicate that Mg NCs can exhibit more favourable thermodynamics (that is, lower enthalpies for hydride formation) than bulk Mg owing to the destabilization of MgH_2 formation[6,7]. Additionally, it is known that the chemical reactivity of Mg NCs positively correlates to the large metal surface area and the short diffusion path of hydrogen[25]. We postulate that

nanostructuring of magnesium in the nanocomposites obviates the need for expensive heavy-metal catalysts by reducing the activation energy for absorption and release of hydrogen[11]. To assess this, we have determined an activation energy (E_a) from analysis of the absorption and release of hydrogen at three different temperatures (Supplementary Fig. S7). We measure E_a values of 25 and 79 kJ mol^{-1} for absorption and desorption, respectively, which are comparable to, and in some cases lower than, those obtained from similar materials requiring the use of heavy-metal catalysts[26].

Hydrogen absorption in a crystalline solid can either occur as a result of isotropic diffusion and random nucleation, or preferential nucleation along certain favourable crystal axes. Further optimization of these materials requires a physical understanding of the mechanism of hydride formation in the nanocomposite, which can be obtained by means of modelling of the uptake kinetics. Here, experimental absorption data of the Mg NCs/PMMA composite materials was fitted with several basic empirical and theoretical kinetic models developed by Avrami[27], which enable characterization of the mechanism and dimensionality of MgH_2 phase formation. Experimental data from the first 6 min of hydrogen absorption in the Mg NCs/PMMA composites was fitted with the Johnson–Mehl–Avrami model (equation (1)):

$$[-\ln(1-\alpha)]^{1/n} = kt \quad (1)$$

where α is the hydrogenated fraction of Mg, k is the phase transformation constant, t is time, and n is the dimensionality of MgH_2 growth. This model assumes a constant interface velocity of MgH_2 formation[21].

By using the dimensionality factor (n) in equation (1) as a fitting parameter, and solving for the best fit (R^2) of the data, the dimensionality of the growth of the MgH_2 phase was determined to be 1.1740 ($R^2 = 0.998$). There exist numerous growth and nucleation scenarios consistent with a value of $n = 1$, including nucleation and growth along one-dimensional (1D) dislocation lines and thickening of cylinders, needles, and plates[28]. We posit that MgH_2 growth in the individual Mg nanocrystals in the composite occurs nearly one-dimensionally along columnar defects as they are exposed to H_2 gas (Fig. 3b), as consistent with the high-resolution TEM (HRTEM) observations (Fig. 2b), although other possible scenarios cannot be excluded at present. To exclude other competing mechanisms, the MgH_2 hydrogen absorption data was fitted to additional Johnson–Mehl–Avrami models of varying dimensionality and mechanism (equations 2–4 in Supplementary Table S2). These additional Johnson–Mehl–Avrami models (Supplementary Fig. S8) had comparatively poor fits ($R^2 =$ 0.914–0.964) compared with the growth model of equation (1), supporting the hypothesis that hydrogen absorption in the Mg NCs/PMMA composites occurs by means of 1D growth. This novel, 1D growth mechanism is also consistent with our measurement of rapid kinetics in the Mg NCs, as hydrogen diffusion through Mg hydride layers is many orders of magnitude slower than the diffusion of hydrogen atoms through lattice vacancies[25,29]. Analysis of HRTEM images of the composites provides evidence for the existence of defects in the Mg NCs (Fig. 2b). It is known that hydrogen atoms can more easily diffuse along 1D line defects, which can act as hydrogen trap sites. Thus, we posit that in Mg NCs/PMMA composites, hydrogen atoms rapidly nucleate and accumulate along these defects and form a metal hydride layer in one dimension, followed by subsequent growth and thickening from the pure metallic core. This conclusion also corroborates recent published results on hydride growth in MgH_2 fibres[19].

In summary, we have developed a new, simple method to synthesize air-stable crystalline Mg NCs/PMMA composites by encapsulation in a polymer with selective gas permeability, protecting the NCs from O_2 and H_2O. The Mg NCs/PMMA composites impressively showed no oxidation in HRTEM diffractograms after two weeks of air exposure. Rapid uptake (<30 min at 200 °C) of hydrogen was achieved with a high capacity (~6 wt% in Mg, ~4% overall) in the absence of heavy-metal catalysts, demonstrating a volumetric capacity (55 g l^{-1}) greater than that of compressed H_2 gas. Theoretical modelling of the experimental data with a Johnson–Mehl–Avrami model indicates that hydrogenation of Mg NCs proceeds through 1D growth, which can occur along line defects in the Mg NCs, as observed by means of HRTEM. On the whole, this approach of synthesizing nanosized air-sensitive metal nanocrystals protected in a gas-selective polymer provides new opportunities in low-cost high-capacity hydrogen storage media, batteries and fuel cells.

Methods

The Mg NCs/PMMA composites were prepared in an inert atmosphere. Bis(cyclopentadienyl)magnesium (Cp_2Mg) (154 mg, 1.00 mmol) was reduced in a solution of tetrahydrofuran (9 ml) containing lithium (9 mg, 1.29 mmol), naphthalene (120 mg, 0.94 mmol), and poly(methyl methacrylate) (60 mg), stirring under Ar atmosphere overnight. The resultant product was isolated by centrifugation, washed with tetrahydrofuran, and dried under an inert atmosphere prior to performing all characterization and measurements. The hydrogenation experiments were performed on the composite samples after first annealing in a helium environment for >24 h to remove solvent and unreacted monomer. The hydrogenation/desorption tests were performed at 200 °C and 35 and 0 bar of H_2 respectively.

Received 5 November 2010; accepted 28 January 2011; published online 13 March 2011

References

1. Jain, I. P., Lal, C. & Jain, A. Hydrogen storage in Mg: A most promising material. *Int. J. Hydrog. Energy* **35,** 5133–5144 (2010).
2. Murray, L. J., Dincă, M. & Long, J. R. Hydrogen storage in metal–organic frameworks. *Chem. Soc. Rev.* **38,** 1294–1314 (2009).
3. Germain, J., Fréchet, J. M. J. & Svec, F. Nanoporous polymers for hydrogen storage. *Small* **5,** 1098–1111 (2009).
4. Patchkovskii, S. *et al.* Graphene nanostructures as tunable storage media for molecular hydrogen. *Proc. Natl Acad. Sci. USA* **102,** 10439–10444 (2005).
5. Schlapbach, L. & Zuttel, A. Hydrogen-storage materials for mobile applications. *Nature* **414,** 353–358 (2001).
6. Cheung, S., Deng, W-Q., van Duin, A. C. T. & Goddard, W. A. $ReaxFF_{MgH}$ reactive force field for magnesium hydride systems. *J. Phys. Chem. A* **109,** 851–859 (2005).
7. Wagemans, R. W. P., van Lenthe, J. H., de Jongh, P. E., van Dillen, A. J. & de Jong, K. P. Hydrogen storage in magnesium clusters: Quantum chemical study. *J. Am. Chem. Soc.* **127,** 16675–16680 (2005).
8. Zahiri, B., Amirkhiz, B. S. & Mitlin, D. Hydrogen storage cycling of MgH_2 thin film nanocomposites catalyzed by bimetallic Cr Ti. *Appl. Phys. Lett.* **97,** 083106 (2010).
9. Aguey-Zinsou, K. F., Ares Fernandez, J. R., Klassen, T. & Bormann, R. Effect of Nb_2O_5 on MgH_2 properties during mechanical milling. *Int. J. Hydrog. Energy* **32,** 2400–2407 (2007).
10. Haas, I. & Gedanken, A. Synthesis of metallic magnesium nanoparticles by sonoelectrochemistry. *Chem. Commun.* 1795–1797 (2008).
11. Li, W., Li, C., Ma, H. & Chen, J. Magnesium nanowires: Enhanced kinetics for hydrogen absorption and desorption. *J. Am. Chem. Soc.* **129,** 6710–6711 (2007).
12. de Jongh, P. E. *et al.* The preparation of carbon-supported magnesium nanoparticles using melt infiltration. *Chem. Mater.* **19,** 6052–6057 (2007).
13. Park, J., Joo, J., Kwon, S. G., Jang, Y. & Hyeon, T. Synthesis of monodisperse spherical nanocrystals. *Angew. Chem. Int. Ed.* **46,** 4630–4660 (2007).
14. Grubbs, R. B. Roles of polymer ligands in nanoparticle stabilization. *Polym. Rev.* **47,** 197–215 (2007).
15. Kalidindi, S. B. & Jagirdar, B. R. Highly monodisperse colloidal magnesium nanoparticles by room temperature digestive ripening. *Inorg. Chem.* **48,** 4524–4529 (2009).
16. Mark, J. E. (ed.) *Polymer Data Handbook* (Oxford Univ. Press, 1999).
17. Min, K. E. & Paul, D. R. Effect of tacticity on permeation properties of poly(methyl methacrylate). *J. Polym. Sci. Polym. Phys.* **26,** 1021–1033 (1988).
18. Bhide, B. D. & Stern, S. A. Permeability of silicone polymers to hydrogen. *J. Appl. Polym. Sci.* **42,** 2397–2403 (1991).
19. Zlotea, C., Lu, J. & Andersson, Y. Formation of one-dimensional MgH_2 nano-structures by hydrogen induced disproportionation. *J. Alloys Compounds* **426,** 357–362 (2006).

20. Moon, H. R., Urban, J. J. & Milliron, D. J. Size-controlled synthesis and optical properties of monodisperse colloidal magnesium oxide nanocrystals. *Angew. Chem. Int. Ed.* **48,** 6278–6281 (2009).
21. Rudman, P. S. Hydrogen-diffusion-rate-limited hydriding and dehydriding kinetics. *J. Appl. Phys.* **50,** 7195–7199 (1979).
22. Vigeholm, B., Kjoller, J. & Larsen, B. Magnesium for hydrogen storage. *J. Less-Common Met.* **74,** 341–350 (1980).
23. Kisielowski, C. *et al.* Detection of single atoms and buried defects in three dimensions by aberration-corrected electron microscope with 0.5-Å information limit. *Microsc. Microanal.* **14,** 469–477 (2008).
24. Danaie, M., Tao, S. X., Kalisvaart, P. & Mitlin, D. Analysis of deformation twins and the partially dehydrogenated microstructure in nanocrystalline magnesium hydride (MgH_2) powder. *Acta Mater.* **58,** 3162–3172 (2010).
25. Dornheim, M., Eigen, N., Barkhordarian, G., Klassen, T. & Bormann, R. Tailoring hydrogen storage materials towards application. *Adv. Eng. Mater.* **8,** 377–385 (2006).
26. Denis, A., Sellier, E., Aymonier, C. & Bobet, J. L. Hydrogen sorption properties of magnesium particles decorated with metallic nanoparticles as catalyst. *J. Alloys Compounds* **476,** 152–159 (2009).
27. Avrami, M. Granulation, phase change, and microstructure—kinetics of phase change. III. *J. Phys. Chem.* **9,** 177–184 (1941).
28. Christian, J. W. *The Theory of Transformations in Metals and Alloys, Part I: Equilibrium and General Kinetic Theory* 2nd edn (Pergamon, 1975).
29. Ragone, D. V. *Thermodynamics of Materials* (Wiley, 1995).

Acknowledgements

Work at the Molecular Foundry and the National Center for Electron Microscopy was supported by the Office of Science, Office of Basic Energy Sciences, of the US Department of Energy under Contract No. DE-AC02-05CH11231. J.J.U., K-J.J., H.R.M., and R.B. are supported under the US Department of Energy Hydrogen Storage Program. A.M.R. is supported as part of the Center for Nanoscale Control of Geologic CO_2, an Energy Frontier Research Center funded by the US Department of Energy, Office of Science, Office of Basic Energy Sciences under Contract No. DE-AC02-05CH11231. We thank J. R. Long and T. J. Richardson for critical discussions and exchange, and appreciate the support of S. Mao for PCI measurement.

Author contributions

J.J.U., K-J.J., and H.R.M. conceived and designed the experiments. K-J.J., H.R.M, A.M.R., and R.B. performed the experiments. K-J.J, B.J. and C.K contributed towards TEM, EELS acquisition and analysis. K-J.J., H.R.M., A.M.R., and J.J.U. analysed the data and wrote the manuscript. All authors discussed the results and commented on the manuscript.

Additional information

The authors declare no competing financial interests. Supplementary information accompanies this paper on www.nature.com/naturematerials. Reprints and permissions information is available online at http://npg.nature.com/reprintsandpermissions. Correspondence and requests for materials should be addressed to J.J.U.